Chapter in **Advancing Astrophysics with the SKA – II**

Exploring Tidal Disruption Events with SKA and VLBI: Unveiling the Mystery of Black Hole Feeding and Outflows

Xinwen Shu[1,†] Guobin Mou[2] Tao An[3] S. Komossa[4] Miguel Pérez-Torres[5,†] Weihua Lei[6] Luming Sun[1] Ning Jiang[3] Tinggui Wang[3] Chichuan Jin[7] and Jun Yang[8]

[1]*Department of Physics, Anhui Normal University, Wuhu, Anhui 241002, China*
[2]*Department of Physics and Institute of Theoretical Physics, Nanjing Normal University, Nanjing 210023, China*
[3]*Department of Astronomy, University of Science and Technology of China, Hefei, Anhui 230026, China*
[4]*Max-Planck-Institut für Radioastronomie, Auf dem Hügel 69, 53121 Bonn, Germany*
[5]*Instituto de Astrofísica de Andalucía, Consejo Superior de Investigaciones Científicas (CSIC), Glorieta de la Astronomía s/n, E-18008, Granada, Spain*
[6]*Department of Astronomy, Huazhong University of Science and Technology, Wuhan 430074, China*
[7]*National Astronomical Observatories, Chinese Academy of Sciences, Beijing 100101, China*
[8]*Onsala Space Observatory, SE-439 92 Onsala, Sweden*
[†]*Chapter co-ordinator*
E-mail: xwshu@ahnu.edu.cn, gbmou@njnu.edu.cn, antao@shao.ac.cn, skomossa@mpifr.de, torres@iaa.csic.es, leiwh@hust.edu.cn

Abstract: Tidal disruption events (TDEs) probe the birth and evolution of black-hole accretion flows and jets on human timescales. Radio emission traces shocks and outflows from non-jetted ("thermal") TDEs and powerful relativistic jets in the rare "jetted" class. SKA-Mid, phased for VLBI and used together with global networks, will deliver sub-mas imaging, tens-of-μas astrometry, and μJy sensitivity, enabling: (i) proper-motion measurements that discriminate off-axis relativistic jets from sub-relativistic winds; (ii) resolved morphologies and magnetic-field diagnostics via polarimetry; and (iii) precise nuclear localization to distinguish SMBH vs. IMBH and to reveal recoil or binary systems. SKA's wide frequency coverage (0.35–15.4 GHz) and 1-h continuum sensitivities of $\approx 3 - 10\mu$Jy beam^{-1}, together with multi-beam tied-array VLBI and a transient buffer for rapid triggers, are transformational. Rubin/LSST, Einstein Probe, and SVOM will increase TDE alerts to tens–hundreds per year, and late-time radio flares appear common ($\gtrsim 40\%$), ensuring rich SKA–VLBI samples. We provide observing strategies, detection forecasts, and predictions (e.g., ≥ 5 proper-motion detections of jetted/off-axis TDEs per year; routine μas-level core-shift constraints). This program will establish TDEs as laboratories for exploring jet launching, particle acceleration (including neutrinos), black hole accretion history and demographics, and properties of circumnuclear medium.

Keywords: Tidal disruption events; Radio jets; Outflows; Circumnuclear medium

1 Introduction

Tidal disruption events (TDEs) represent a captivating intersection of astrophysics, occurring when a star is drawn too close to a supermassive black hole (SMBH) and is torn apart by tidal forces (Rees, 1988), producing bright, multi-wavelength flares (Gezari, 2021; Komossa, 2015). These events provide a unique opportunity to study black hole feeding mechanisms, accretion processes, outflows, relativistic jets, and the environments surrounding SMBHs (An et al., 2026, in this Book). The Square Kilometre Array (SKA), in conjunction with Very Long Baseline Interferometry (VLBI), offers unprecedented capabilities to investigate the radio emissions associated with TDEs, addressing key questions in the field:

(1) Jet formation and evolution: Incipient jet kinematics (proper motion via VLBI) and spectral energy distribution (SED) evolution during the emergent phase. The prospects of using SKA+VLBI to address this question will be presented in Sections 2, 3, 5 and 7.

(2) Delayed Emission Physics: Temporal correlation between accretion-state transitions (e.g., disk-jet coupling timescales) traced by optical and X-ray observations, and delayed radio flares via high-cadence multi-epoch monitoring. The unique role of SKA+VLBI observations in uncovering the origins of delayed radio flares will be presented in Section 3.

(3) Properties of circumnuclear medium (CNM): Statistical constraints on the CNM inhomogeneities at scales of (sub-)parsecond (pc), through population-level outflow-CNM interaction studies (in comparison with dedicated hydrodynamic simulations). SKA+VLBI observations will enable to diagnose the properties of smooth CNM and dense clouds (Section 4).

(4) Demographic Completeness: Unbiased detection of rare TDE subtypes (high-z events, off-axis jets, and systems involving intermediate-mass black hole (IMBH) and SMBH binary (SMBHB)) across diverse host galaxy environments. The scientific applications of SKA+VLBI for unbiased detections of TDEs will be presented in Section 5.

(5) Multi-messenger Associations: Understanding the driving mechanisms that produce the high energy neutrinos in TDEs. SKA+VLBI observations are able to localize precisely the radio emitting region and place a rigorous constraint on the energetics relevant to the production of neutrinos (Section 6).

2 Relativistic jet formation and evolution

2.1 Background

The condition for relativistic jet formation and its connection with accretion onto SMBHs is largely unclear. Stellar TDE by SMBH lead to dramatic changes in accretion rate by orders of magnitude (e.g., Rees, 1988; Komossa, 2015), presenting a unique laboratory to study jet formation. Despite more than a hundred TDEs discovered so far, only four have been observed to launch relativistic jets; three are discovered in the hard X-rays, including Swift J1644+5734 (Burrows et al., 2011) , Swift J2058.4+0516 (Cenko et al., 2012), and Swift J1112-8238 (Brown et al., 2015), and one in the optical, AT2022cmc (Andreoni et al., 2022). Jetted TDEs could be misidentified as long

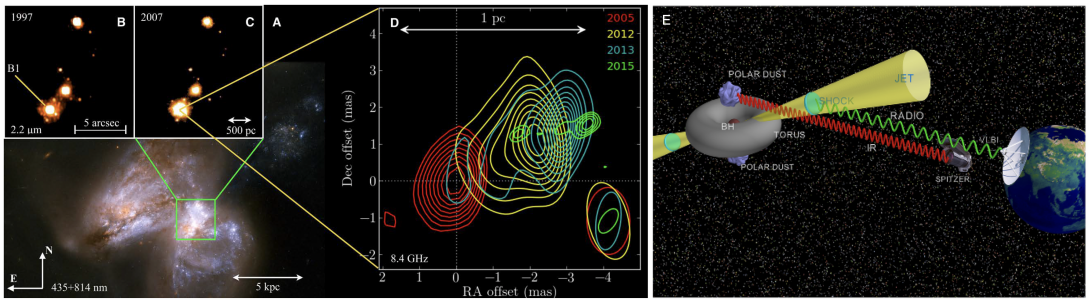

Figure 1: The left panels show the near-infrared outburst of the TDE Arp 299-B AT1 (**B** and **C**) and the color-composite optical image of its host galaxy (**A**). The evolution of the radio morphology as imaged with VLBI at 8.4 GHz (Mattila et al., 2018) is shown in panel **D**. It can be seen that an initially unresolved radio source develops into a resolved jet structure a few years after the explosion, which is viewed with a slightly off-axis angle ($\theta_{\rm obs} = 25^\circ - 35^\circ$, **E**).

Gamma-ray bursts (GRBs) or X-ray flashes (Tchekhovskoy et al., 2014; Shu et al., 2025; Li et al., 2026), making the true abundance of jetted TDEs largely uncertain. In addition, it remains puzzling why only a small fraction (<1%) of TDEs launch successful jets. Possible explanations include that jet formation requires special conditions on the SMBH spin and magnetic field (e.g., Tchekhovskoy et al., 2014), the jet is chocked by the disk wind in most TDEs (Teboul and Metzger, 2023; Lu et al., 2024), or the large off-axis viewing angle of jet (Matsumoto and Piran, 2023). However, the limited data on jetted TDEs prevents adequate testing of these explanations.

2.2 SKA-VLBI capability, observing strategy, and expected results

All four on-axis jetted TDEs exhibit luminous ($\nu L_\nu > 10^{40}$ erg s^{-1}) and long-lived radio emission. However, no apparent superluminal motion has been detected in the known jetted TDEs with VLBI observations at a resolution of ~1 mas, such as Swift J1644+5734 (Yang et al., 2016), possibly due to a very small viewing angle, a strong jet deceleration, or a too small physical scale. With the VLBI observations over a decade, Mattila et al. (2018) reported the discovery of a resolved and expanding radio jet ($\beta \approx 0.3$c) in the dust-enshrouded TDE Arp 299-B AT1 at $z = 0.01$, likely originating from a jet viewing slightly off-axis ($\theta_{\rm obs} = 25^\circ - 35^\circ$, Figure 1).

The two high-energy instruments aboard the Space Variable Objects Monitor (SVOM; Wei et al., 2016) space mission, the ECLAIRs and GBM (4-150 keV and 15-5000 keV, respectively) are characterized by a large field of view and are optimally suited for the detection of new jetted TDEs. The space mission Einstein Probe (EP; Yuan et al., 2025) will additionally detect soft X-ray TDEs that may launch relativistic radio-emitting outflows. Both missions stand out due to their rapid alert time after the discovery of new transients within minutes, ensuring quick follow-ups in the radio regime and therefore probing the very early phases of jet launching. Radio follow-ups of extraordinary bright TDEs discovered in time-domain X-ray surveys from SVOM and EP, optical surveys from LSST, or directly by radio surveys with SKA have the potential to resolve jet emission and probe the dynamics of jet evolution, especially in the early ultra-relativistic phase.

Over its past one-year operation, EP has detected a few jetted TDE candidates in real time (Shu et al., 2025; Li et al., 2026). We anticipate that at least 1-2 jetted TDEs per year would be detected

in the coming LSST, EP and SVOM surveys, which are ideal targets for follow-up observations by SKA+VLBI. SKA-Mid Bands 2 (0.95–1.76 GHz) and 5 (4.6–15.4 GHz) provide the critical SKA+VLBI frequency coverage for size measurements and astrometry studies. The intercontinental baselines imply a spatial resolution of $\theta_{\rm beam} \simeq \lambda/B_{\rm max} \approx$1 mas at 8 GHz and ≈0.5 mas at 15 GHz. The naturally weighted map *rms* for a global multi-baseline imaging including SKA-Mid reaches a few μJy/beam, e.g., ∼3μJy/beam in ∼1 hour integration, depending on the actual antennas in operation and processed bandwidth. The positional uncertainties of $\sigma_{\rm pos} \approx \theta_{\rm beam}/(2 \times {\rm SNR})$, where SNR is the signal-to-noise ratio, suggest that tens of μas relative astrometry can be achieved for mJy-level sources. Once triggered as jetted TDE candidates from optical and X-ray surveys, we envisage that the SKA observations in commensal mode during the first a few days of evolution will determine whether the radio flare is detectable or not. If the target is bright enough in the SKA-Mid bands (i.e., $\gtrsim$ 0.5 mJy), 3-4 long ($\gtrsim$ 8 h) SKA+VLBI tracks can be scheduled, spanning a few weeks to months post trigger. For jetted TDEs at z $\lesssim$ 0.1, SKA+VLBI will enable to directly resolve the radio emission components at pc scales, or measure the proper motion, providing a compelling evidence for the presence of a radio jet. In addition, multi-frequency SKA+VLBI observations, especially at Bands 5a and 5b, will provide the precise position (tens of μas astrometry) of the compact core as a function of observing frequency. The measured offset between frequency pairs yields a core-shift parameter, which can be used to estimate the magnetic field strength of the jet-emitting region (e.g., Sokolovsky et al., 2011). The core-shift-derived magnetic field strength will be important to understand the physical conditions for jet launching.

3 Delayed emission physics and non-relativistic outflows

In comparison with jetted TDEs, radio emission from thermal TDEs has lower luminosities, possibly dominated by non-relativistic outflows. Thermal TDEs refer to those flares in optical/UV and X-rays that can be described by a blackbody emission, which is distinct from the non-thermal emission from jetted TDEs. The low-luminosity radio emission in thermal TDEs appears to be ubiquitous (Alexander et al., 2016) . Recently, Cendes et al. (2024) present the results from radio follow-up observations of 23 optical TDEs and find that ∼ 40% of them exhibit radio brightening hundreds to thousands of days after the discovery. The nature of the late-time radio brightening in TDEs is still under debate, and several scenarios have been proposed, including decelerating and expansion of an off-axis jet launched at the time of disruption (e.g., Matsumoto and Piran, 2023), a delayed launching of the outflow perhaps from delayed disk formation (Horesh et al., 2021; Cendes et al., 2024), changes in the structure and density profile of CNM (e.g., Mou et al., 2022; Matsumoto and Piran, 2024), and break out of the choked precessing jets from the wind envelop (Teboul and Metzger, 2023; Lu et al., 2024).

VLBI observations will be able to test directly the scenario of an off-axis jet for the origin of delayed radio flares. In the off-axis scenario, assuming that the relativistic jet travels roughly perpendicularly to our line of sight at the speed of light for a typical TDE at a distance of ∼100 Mpc, the proper motion of the radio source is ∼0.6 mas/year. We propose to use SKA+VLBI Band 5 to observe a sample of optical and/or X-ray thermal TDEs with late-time radio brightening, especially those with steeply rising light curves (e.g. Cendes et al., 2022). 3-4 long ($\gtrsim$ 8 h) SKA+VLBI observations

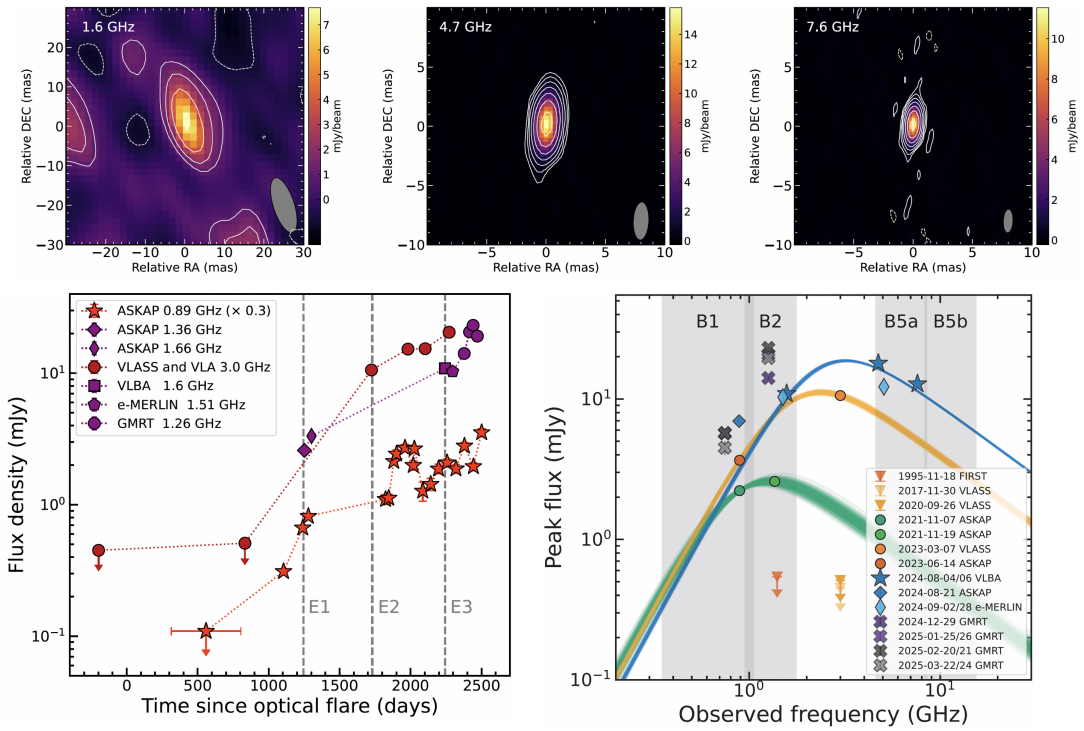

Figure 2: Natural-weighted images of VLBA observations of AT2018cqh at three frequencies (upper panel), which reveal a compact radio emission, unresolved at a scale of $\lesssim 0.13$ pc (Yang et al., 2025). Lower panel shows the radio light curves at 0.89 GHz, 1.3-1.6 GHz and 3 GHz (left), and the radio SEDs over three epochs (right). The green, orange, and blue lines represent the best fits to each SED, which are the model realizations of MCMC fittings. The shaded regions represent the frequency range covered by SKA-Mid. There is a steady rise in both the peak flux density and frequency between the three epochs, which have rarely been observed in TDEs.

over ∼1-3 years will enable to measure the proper motion since the rise in radio emission, hence place an useful constraint on the off-axis scenario. If this scenario is confirmed, it implies that the jet has a very large energy of $\gtrsim 10^{52}$ erg (Beniamini et al., 2023; Matsumoto and Piran, 2023), which will have interesting implications for the total energy released and provide new clues to resolve the "missing energy" puzzle in TDEs (Lu and Kumar, 2018). Alternatively, a null result will rule it out, and favor the scenario of late launch of an outflow (Figure 2). On the other hand, VLBI observations are also crucial to constrain the CNM properties, for which we will discuss in more detail in next Section, by comparing with hydrodynamic simulations of the interaction of outflow with CNM and/or dense clouds.

4 Properties of the circumnuclear medium

4.1 Background

The origin of radio emissions in TDEs remains an open question in high-energy astrophysics. In most cases, radio emissions are thought to be generated by the forward/external shocks (FS) driven by outflow in the ambient CNM, while rare cases are thought to originate from internal shocks

within the jet (Alexander et al., 2020; Pasham and van Velzen, 2018). In such a forward shock scenario, using the multi-frequency data, one can fit the radio spectrum and determine the peak frequency ν_p and peak flux F_{ν_p}. Following the energy equipartition method (Barniol Duran et al., 2013), the size of the radiative zone and the total nonthermal energy and be calculated, which can be further used to estimate the radius and total amount of post-shock gas. Accordingly, the CNM density at different radii can be derived. Therefore, the radio emissions at different epochs can be used to construct the CNM density profile at pc or even sub-pc scales (Alexander et al., 2016; Zhou et al., 2024).

4.2 Smooth CNM and dense clouds

Recent radio observations have uncovered the diversity of radio afterglows in TDEs. An increasing number of radio afterglows exhibit a sharply rising flux and some show a derived shock radius that changes little with time when applying the FS model (e.g., Yang et al. 2025). These features challenge the conventional FS model but are consistent with the bow shock (BS) model, in which the radio emission is produced by BS formed as the outflow impacts high-density gas. These findings suggest that BS and dense gas could exist in some TDEs, and more importantly, confirm that radio observations can be used to investigate the circumnuclear environment in galactic nuclei and to explore simultaneously the diffuse CNM and dense gas.

On the other hand, the CNM density profile ($n \propto R^{-k}$) provides key diagnostics of the accretion history of the SMBH. Currently, there are three special types of CNM density profiles: (1) Sgr A*-like ($k = 1$), namely, the CNM density profile consistent with Sgr A* whose $k = 1$ (Baganoff et al., 2003), and AT2019dsg is one of the TDEs satisfying this distribution (Stein et al., 2021); (2) Bondi-like ($k = 3/2$), consistent with Bondi accretion whose $k = 3/2$, and Sw J1644+57 is one of the TDEs satisfying this distribution (Eftekhari et al., 2018); (3) ASASSN-14li-like ($k = 5/2$), there are several TDEs satisfying this distribution, such as ASASSN-14li (Alexander et al., 2016), CNSS J0019+00 (Anderson et al., 2020) and Arp 299-B AT1 (Mattila et al., 2018). Such a steep profile is not expected for spherically symmetric accretion, but appears in some models of super-Eddington accretion flows (Coughlin and Begelman, 2014, ZEBRAs).

4.3 Hydrodynamic simulations

Hydrodynamic simulations are crucial to understand the delayed physical process in the interaction of outflow with CNM and/or clouds. The high-energy electrons and magnetic fields in the FS are dispersed throughout the post-shock CNM, resulting in a relatively large spatial distribution region. Compared to the FS, the high-energy electrons and magnetic fields in the BS are concentrated at the shock front (the windward side of the cloud). These discrepancies lead to different spectra and temporal evolution of the radio emission from the BS compared to the FS. Recent two-fluid simulations incorporating the relativistic electrons as the second fluid have revealed the light curve patterns and spectral characteristics for both FS and BS, and prove the significant differences between these two types of shocks (Mou, 2025; Mou and Shu, 2025, under review). For light curves at high frequencies ($\nu > \nu_p$), the flux variation of the FS is relatively gradual. In contrast, the flux of the BS rises sharply with the onset of cloud impact and then declines rapidly as the interaction ends. The radio flux from the BS could exhibit short-term (monthly) variations when

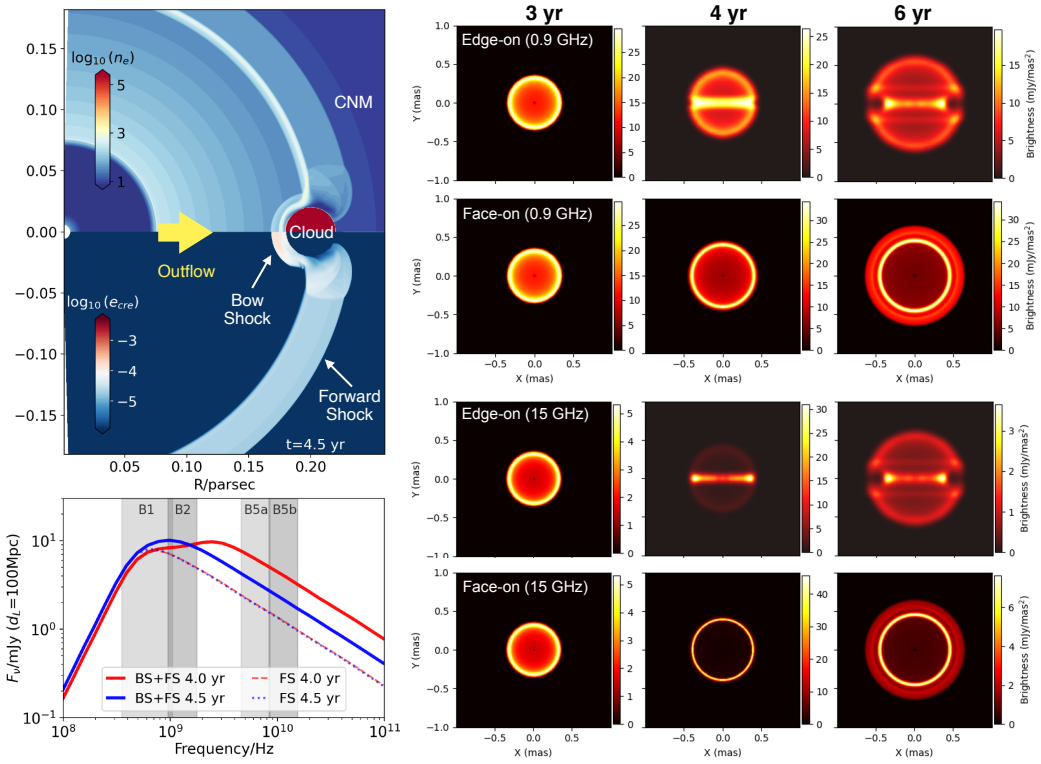

Figure 3: The left panels show the snapshots of gas density and energy density of relativistic electrons during the outflow-CNM/cloud interaction (in Gaussian-cgs units), as well as the synthetic radio spectra (d_L = 100 Mpc). The spectral panel displays both the BS+FS component and the FS component alone, from which the impact and the rapid variability feature of the BS can be observed. The shaded regions represent the frequency range covered by SKA-Mid. The right panels show the synthetic radio maps, with axes labeled in milliarcseconds. The three epochs correspond to the phases before the BS emerges (3 yr, when only the forward shock is present), the early stage (4 yr) and the late stage (6 yr) of the outflow-cloud interaction (Mou and Shu, 2025, under review).

the outflow exhibits short-term fluctuations, while for the FS, its radio emission is hard to produce noticeable fluctuations on a timescale of months. The overall radio spectra are determined by both shocks, when they coexist in a certain source. When BS's contribution is significant, it could form double-peaked or flat-top features in spectra (Figure 3, left). Note that the flux displayed in the bottom left panel is calculated for d_L = 100 Mpc. With its extraordinary high sensitivity, SKA will be powerful in discovering more radio afterglows at a flux level of $\lesssim 50\mu$Jy and characterizing the light curves and spectral evolution. These data will facilitate the studies on the origins of the radio emission, enable the identification of BS and clouds, and thereby reveal the circumnuclear environment in which the radio afterglows occur. In the case of BS, we can use the radio flux and spectral evolution to map the properties of gaseous clouds at a sub-pc scale (e.g., Yang et al., 2025), which cannot be probed via direct measurements even in the nearest supermassive black holes.

On the other hand, for nearby TDEs (d_L < 100 Mpc), high-resolution SKA+VLBI observations can distinguish the radio structure and help to directly identify the presence of a BS. We examined the case for an isotropic outflow with a velocity of 0.2 c impacting both a toroidal cloud (assuming

to locate at 0.2 pc from the SMBH with a radius of 0.02 pc and a covering factor of 10%) and a hot diffuse CNM with a Sgr A*-like density profile (Gillessen et al., 2019). Figure 3 shows the synthetic radio images at various times and viewing angles (assuming at d_L = 100 Mpc and d_A = 96 Mpc). The FS radio emission clearly expands over time, while the BS appears as stationary bright spots (in edge-on views) or a bright ring (in face-on views). Such imaging differences can also be used to determine the origin of the radio emission. Note that the radio flux density in our simulations from both bow shock and forward shock depends on the parameters for outflow, smooth CNM and dense clouds, and the actual flux can be lower than that shown in Figure 3. For most radio-emitting TDEs, with a spatial resolution of ~0.5 mas at Band 5b, SKA+VLBI observations over a period of 3-5 years are able to resolve the radio emission of FS from BS (Figure 3, right).

5 Unbiased detection of TDEs across diverse host galaxy environments

Optical TDEs preferentially occur in post-starburst galaxies (French et al., 2016). However, whether there are equally high TDE rates in star-forming and starburst galaxies remains unclear. Although optical surveys rarely detect TDEs in starforming galaxies (e.g., Yao et al., 2023), this might be caused by dust obscuration (Roth et al., 2021) and the intrinsic TDE rate may be high (Tadhunter et al., 2017). To obtain an unbiased TDE demography, it is necessary to probe TDEs in the mid-infrared and radio bands with weak dust extinction. Although some candidates of obscured TDEs have been discovered in these bands (Jiang et al., 2021; Somalwar et al., 2022; Masterson et al., 2024), their nature is still under debate. The mid-infrared flare of Arp 299-B AT1 (Mattila et al., 2018) provides an example of how to probe the TDE nature through VLBI observations, which allow for detecting and measuring the jet proper motion (Figure 1). The jet inclination is different from the axis of pre-existing accretion disk, indicating that the accreted material comes from high-inclination orbits, which strongly favors the TDE scenario. Using Arp 299-B AT1 as a prototype, long-term SKA+VLBI Band 5 observations of optically-dark infrared flares will help to identify more obscured TDEs by measuring the jet orientation and proper motion, uncovering the missing population of TDEs that occurred in starforming and starburst galaxies.

5.1 Identification of off-nuclear TDEs

Off-nuclear TDEs are expected in at least two contexts: (i) disruptions by IMBHs residing in nuclear star clusters, dwarf galaxies, or stripped nuclei; and (ii) disruptions by SMBHs that have been displaced from the galactic center by gravitational-wave recoil or three-body interactions during a merger. Both channels are already hinted at observationally (Yao et al., 2025; Jin et al., 2025, under review) and they open a new window on black hole demographics and studies of galaxy assembly.

The unique combination of high sensitivity (μJy) and spatial resolution (sub-mas) offered by SKA+VLBI will allow a variety of applications related to off-nuclear TDEs. First, off-nuclear TDEs involving IMBHs are expected to form in nuclear star clusters. Given the typical dimensions of nuclear starbursts of up to a few 100 pc (Prieto et al., 2024), these systems will be easily resolved with SKA+VLBI across a broad redshift range. Further, dwarf galaxies with IMBHs frequently reside in galaxy halos. In that case, SKA+VLBI type resolution will be able to spatially resolve

these systems out to much higher redshifts than is possible in the X-ray regime where some such systems have been detected so far (Lin et al., 2020; Li et al., 2026; Jin et al., 2025, under review), and thus will probe aspects of cosmic evolution as well. Second, the rate of TDEs is enhanced in the course of recoiling SMBHs that pass through the dense galactic environments (Komossa and Merritt, 2008). Even if the galaxy's central region is obscured, radio observations will still penetrate the gas and dust and will provide an accurate measurement of the location of the recoiling SMBH within the nucleus (Mattila et al., 2018; Yao et al., 2025). Even if only a few radio jets from recoiling SMBHs can be identified, this will constitute a huge advancement of this new field of research.

Practical confirmation requires VLBI astrometry tied to the host nucleus. Phased SKA-Mid plus global VLBI deliver sub-mas imaging and $\lesssim$ tens-of-μas relative astrometry in $\sim$ 1 h on-source time (rms of $\sim$3–10 μJy beam^{-1}), enabling to secure nuclear-offset measurements and multi-epoch tests for proper motion or expanding ejecta. Dual phase centres (transient + nucleus) mitigate registration systematics. In addition, high brightness temperatures ($> 10^7$ K), evolving synchrotron peaks, and polarimetry/rotation measure mapping are helpful to distinguish cluster/halo environments from nuclear screens. Triggers from Rubin/LSST, EP and SVOM will also provide the chance to capture early offsets and centroid motion of transient radio emission from a newly launched jet.

5.2 Observations of radio emission from TDE candidates by supermassive black hole binaries

Jetted TDEs are an excellent probe of binary SMBHs. In particular, they trace SMBH binaries even in quiescent galaxies without a permanent accretion disk. Such binary SMBHs are otherwise very challenging to detect, as most search methods require at least one SMBH to be active (Komossa and Grupe, 2024). The lightcurve of a jetted TDE in a binary SMBH system will look characteristically different from a TDE in a single SMBH system (Liu et al., 2009): due to the influence of the secondary SMBH on the tidal stream towards the primary, accretion is temporarily interrupted and then restarts, leading to phases of characteristic dips and recoveries in the accretion lightcurve (Liu et al., 2014; Shu et al., 2020). These then affect the jet (if present) accordingly. That method alone is an important future SKA application (An et al., 2026; D'Amato et al., 2026, in this Book).

In practice, phased SKA-Mid plus global VLBI can test the TDE scenario involving SMBHB through time-variable, frequency-dependent jet geometry and astrometry: (i) periodic swings in core position angle and the electric vector polarization angle (precession); (ii) quasi-periodic core-shift cycles across Bands 2–5b tied to modulated jet power; (iii) curved or oscillatory proper motions of compact knots; and (iv) rotation-measure sign changes expected from a precessing helical field. Monthly–quarterly monitoring over 1–3 yr with sub-mas imaging and $\lesssim$ tens-of-μas relative astrometry at μJy sensitivities will separate binary-driven precession from single-BH Lense-Thirring disk precession and from stochastic variability, especially when combined with optical/X-ray dip–and–recovery light curves that flag stream interruptions. These capabilities follow from the SKA+VLBI performance and band coverage summarized for AA*/AA4. On the other hand, if the binary SMBH was itself active and hosting a large-scale jet, then SKA+VLBI observations can additionally be used to trace the jet precession of the large-scale jet, providing unique novel tool of characterizing the binary SMBH orbital parameters.

6 Uncovering the physics of the TDE-neutrinos association

TDEs are inherently multiwavelength and multimessenger sources (e.g., Komossa, 2015). In a variety of situations, the radio regime provides unique information that is either linked to questions of jet formation and evolution, and/or to the high-precision spatial localization of the TDE, or even TDE identification in heavily obscured environments where optical and X-ray detection methods fail. In addition, high-sensitivity radio observations are an important ingredient in the multi-messenger approach: jetted TDEs are candidates for neutrino emitters (Stein et al., 2021; Mohan et al., 2022), and they trace a parameter space very different from blazars: the majority of TDEs are identified in quiescent host galaxies, implying a pristine environment without any previous large- or small-scale jet activity. Further, the presence and properties/configuration of magnetic fields are expected to be different in TDEs that form a compact accretion disk within a short amount of time. It is also suggested that the efficiency of high-energy neutrino production in TDEs could be increased compared to non-flaring active galactic nuclei (AGN), possibly due to the high Eddington ratio of the TDE flares (van Velzen et al., 2024). These aspects make neutrino and radio observations of TDE jets important tracers of jet physics in a unique parameter space. On the other hand, if a TDE occurs in a gas-rich environment with dense clouds at a sub-pc scale (Section 4.2), the outflow-cloud interactions may form shock waves which generate accelerated protons, and hence delayed neutrinos from hadronic interactions in clouds (Wu et al., 2022; Zhou et al., 2026). However, the predicted neutrino number in such a scenario depends on various parameters such as the density and size of the clouds, the covering factor of BS, and shock acceleration efficiency, which cannot be measured directly, even for the nearest TDEs, but could be constrained with radio observations. As suggested by Zhou et al. (2026), the scenario of outflow-cloud interaction in producing the neutrino emission through pp collisions can be tested with future identifications of radio transients coincident with high-energy neutrinos.

Therefore, beyond electromagnetic diagnostics, SKA+VLBI can critically test the emerging TDE–neutrino connection. Hadronic models predict high-energy neutrinos from pγ/pp interactions in jetted or shock-powered TDE outflows, with peak production contemporaneous with the radio-bright phase. Sub-mas imaging and $\lesssim$tens-of-μas (relative) astrometry will localize the synchrotron zone with respect to the nucleus, measure core-shift magnetic fields, and provide kinetic-energy and density calorimetry needed to infer neutrino efficiencies. Rapid targets of opportunity observations to IceCube/KM3NeT/Baikal-GVD EHE/Gold alerts, plus stacking of radio-selected TDE samples, can confirm or refute event-level associations (e.g., AT2019dsg, AT2019fdr and SDSS J1513+3111) and distinguish hadronic from leptonic power. A coordinated program (Bands 2–5b, monthly cadence) will set population-level limits on the TDE contribution to the diffuse neutrino background (e.g., Murase and Waxman 2016; Stein et al. 2021; Reusch et al. 2022).

7 SKA-VLBI observations of transient jet/outflows from other types of SMBH accretion flares

In addition to TDEs, another recent advance in time-domain studies is the identifications of non-regular extreme variability in active galaxies, which can change their optical types on timescales of years, characterized by emerged or disappeared broad emission lines as well as dramatic continuum

variations (e.g., Shappee et al., 2014). This class of "changing-look" AGN (CLAGNs), may even be transitioning between radiatively inefficient and radiatively efficient modes of accretion (Ruan et al., 2019), analogous to X-ray spectral state transitions observed in stellar-mass BHs. On the other hand, there is a new class of flares from accreting SMBHs in AGNs that decline more slowly than normal TDEs, perhaps arising from a longer-term event of intensified gas accretion (Trakhtenbrot et al., 2019a). Another class of SMBH-related accreting flares exhibit characteristics of both AGNs and TDEs, which cannot easily be classified into either source class and have been dubbed as ambiguous nuclear transients (Neustadt et al., 2020; Hinkle et al., 2022). Radio observations of these SMBH-related accreting flares are important to disclose the connection between SMBH accretion and the launching of jets and outflows in a possibly different parameter space from TDEs.

The AGN 1ES 1927+654 is one of few extreme CLAGNs observed to change in the black hole's accretion states in real time (Trakhtenbrot et al., 2019b), which could be triggered by the interaction between the preexisting accretion disk and the fallback debris from TDE (Ricci et al., 2020). Approximately 1800 days after the initial CL event, a significant radio brightening was observed in 1ES 1927+654, consistent with a newly launched radio-emitting outflow. At the resolution of ~0.5 mas, VLBA imaging shows bipolar radio extensions of similar brightness separated by approximately 0.45 mas or 0.15 pc, with a tentative expansion of separation speed of ~0.3c (Meyer et al., 2025). Future wide-field SKA slow-transient surveys will be sensitive enough to capture the transient radio brightening following the AGN flares. We advocate a SKA+VLBI program at Band 5 to track a sample of 10-20 extreme AGN flares similar to 1ES 1927+654, with 3-4 epochs per source spanning a few weeks to years after the discovery, which are necessary to catch the newly launched radio-emitting outflow or monitor its temporal evolution. With improved sensitivity and spatial resolution, SKA+VLBI will enable to detect the resolved jet structures for AGN flares at a distance of $\lesssim$ 100 Mpc, allowing for more detailed studies on the kinematics and energetics of the jet in its earliest evolution phases.

Acknowledgments: We thank the anonymous reviewer for detailed and insightful comments that helped to improve the chapter significantly. LWH acknowledges support from the National Natural Science Foundation of China (grant Nos. 12473012). MPT acknowledges financial support from the Severo Ochoa grant CEX2021-001131-S and from the Spanish grant PID2023-147883NB-C21, funded by MCIU/AEI/ 10.13039/501100011033, as well as support through ERDF/EU. X.S. acknowledges support from the National Science Foundation of China through grant No. 12192220 and 12192221.

References

K. D. Alexander et al. *ApJL*, 819(2):L25, Mar. 2016. doi: 10.3847/2041-8205/819/2/L25.

K. D. Alexander, S. van Velzen, A. Horesh, and B. A. Zauderer. *Space Sci. Rev.*, 216(5):81, June 2020. doi: 10.1007/s11214-020-00702-w.

T. An et al. In *Advancing Astrophysics with the SKA – II (AASKAII)*. 2026. arXiv search: Report number AASKAII/TaoAn03.

M. M. Anderson et al. *ApJ*, 903(2):116, Nov. 2020. doi: 10.3847/1538-4357/abb94b.

I. Andreoni et al. *Nature*, 612(7940):430–434, Dec. 2022. doi: 10.1038/s41586-022-05465-8.
F. K. Baganoff et al. *ApJ*, 591(2):891–915, July 2003. doi: 10.1086/375145.
R. Barniol Duran, E. Nakar, and T. Piran. *ApJ*, 772(1):78, July 2013. doi: 10.1088/0004-637X/772/1/78.
P. Beniamini, T. Piran, and T. Matsumoto. *MNRAS*, 524(1):1386–1395, Sept. 2023. doi: 10.1093/mnras/stad1950.
G. C. Brown et al. *MNRAS*, 452(4):4297–4306, Oct. 2015. doi: 10.1093/mnras/stv1520.
D. N. Burrows et al. *Nature*, 476(7361):421–424, Aug. 2011. doi: 10.1038/nature10374.
Y. Cendes et al. *ApJ*, 938(1):28, Oct. 2022. doi: 10.3847/1538-4357/ac88d0.
Y. Cendes et al. *ApJ*, 971(2):185, Aug. 2024. doi: 10.3847/1538-4357/ad5541.
S. B. Cenko et al. *ApJ*, 753(1):77, July 2012. doi: 10.1088/0004-637X/753/1/77.
E. R. Coughlin and M. C. Begelman. *ApJ*, 781(2):82, Feb. 2014. doi: 10.1088/0004-637X/781/2/82.
Q. D'Amato et al. In *Advancing Astrophysics with the SKA – II (AASKAII)*. 2026. arXiv search: Report number AASKAII/DAmato01.
T. Eftekhari et al. *ApJ*, 854(2):86, Feb. 2018. doi: 10.3847/1538-4357/aaa8e0.
K. D. French, I. Arcavi, and A. Zabludoff. *ApJL*, 818(1):L21, Feb. 2016. doi: 10.3847/2041-8205/818/1/L21.
S. Gezari. *ARA&A*, 59:21–58, Sept. 2021. doi: 10.1146/annurev-astro-111720-030029.
S. Gillessen et al. *ApJ*, 871(1):126, Jan. 2019. doi: 10.3847/1538-4357/aaf4f8.
J. T. Hinkle et al. *ApJ*, 930(1):12, May 2022. doi: 10.3847/1538-4357/ac5f54.
A. Horesh, S. B. Cenko, and I. Arcavi. *Nature Astronomy*, 5:491–497, May 2021. doi: 10.1038/s41550-021-01300-8.
N. Jiang et al. *ApJSS*, 252(2):32, Feb. 2021. doi: 10.3847/1538-4365/abd1dc.
C. C. Jin et al. *arXiv e-prints*, art. arXiv:2501.09580, Jan. 2025. doi: 10.48550/arXiv.2501.09580.
S. Komossa. *Journal of High Energy Astrophysics*, 7:148–157, Sept. 2015. doi: 10.1016/j.jheap.2015.04.006.
S. Komossa and D. Grupe. *Serbian Astronomical Journal*, 209:1–24, Dec. 2024. doi: 10.2298/SAJ2409001K.
S. Komossa and D. Merritt. *ApJL*, 683(1):L21, Aug. 2008. doi: 10.1086/591420.
D. Y. Li, J. Yang, W. D. Zhang, and the Einstein Probe collaborations. *Science Bulletin*, 71(3):538–546, Feb. 2026. doi: 10.1016/j.scib.2025.12.050.
D. Lin et al. *ApJL*, 892(2):L25, Apr. 2020. doi: 10.3847/2041-8213/ab745b.
F. K. Liu, S. Li, and X. Chen. *ApJL*, 706(1):L133–L137, Nov. 2009. doi: 10.1088/0004-637X/706/1/L133.
F. K. Liu, S. Li, and S. Komossa. *ApJ*, 786(2):103, May 2014. doi: 10.1088/0004-637X/786/2/103.
W. Lu and P. Kumar. *ApJ*, 865(2):128, Oct. 2018. doi: 10.3847/1538-4357/aad54a.
W. Lu, T. Matsumoto, and C. D. Matzner. *MNRAS*, 533(1):979–993, Sept. 2024. doi: 10.1093/mnras/stae1770.
M. Masterson et al. *ApJ*, 961(2):211, Feb. 2024. doi: 10.3847/1538-4357/ad18bb.
T. Matsumoto and T. Piran. *MNRAS*, 522(3):4565–4576, July 2023. doi: 10.1093/mnras/stad1269.
T. Matsumoto and T. Piran. *ApJ*, 971(1):49, Aug. 2024. doi: 10.3847/1538-4357/ad58ba.
S. Mattila et al. *Science*, 361(6401):482–485, Aug. 2018. doi: 10.1126/science.aao4669.
E. T. Meyer et al. *ApJL*, 979(1):L2, Jan. 2025. doi: 10.3847/2041-8213/ad8651.

P. Mohan et al. *ApJ*, 927(1):74, Mar. 2022. doi: 10.3847/1538-4357/ac4cb2.

G. Mou. *arXiv e-prints*, art. arXiv:2510.14715, Oct. 2025.

G. Mou and X. Shu. *arXiv e-prints*, art. arXiv:2510.25033, Oct. 2025.

G. Mou, T. Wang, W. Wang, and J. Yang. *MNRAS*, 510(3):3650–3657, Mar. 2022. doi: 10.1093/mnras/stab3742.

K. Murase and E. Waxman. *Phys. Rev. D*, 94(10):103006, Nov. 2016. doi: 10.1103/PhysRevD.94.103006.

J. M. M. Neustadt et al. *MNRAS*, 494(2):2538–2560, May 2020. doi: 10.1093/mnras/staa859.

D. R. Pasham and S. van Velzen. *ApJ*, 856(1):1, Mar. 2018. doi: 10.3847/1538-4357/aab361.

A. Prieto et al. *MNRAS*, 533(1):433–454, Sept. 2024. doi: 10.1093/mnras/stae1822.

M. J. Rees. *Nature*, 333(6173):523–528, June 1988. doi: 10.1038/333523a0.

S. Reusch et al. *Phys. Rev. Let.*, 128(22):221101, June 2022. doi: 10.1103/PhysRevLett.128.221101.

C. Ricci et al. *ApJL*, 898(1):L1, July 2020. doi: 10.3847/2041-8213/ab91a1.

N. Roth, S. van Velzen, S. B. Cenko, and R. F. Mushotzky. *ApJ*, 910(2):93, Apr. 2021. doi: 10.3847/1538-4357/abdf50.

J. J. Ruan et al. *ApJ*, 883(1):76, Sept. 2019. doi: 10.3847/1538-4357/ab3c1a.

B. J. Shappee et al. *ApJ*, 788(1):48, June 2014. doi: 10.1088/0004-637X/788/1/48.

X. Shu et al. *Nature Communications*, 11:5876, Nov. 2020. doi: 10.1038/s41467-020-19675-z.

X. Shu et al. *ApJL*, 990(1):L29, Sept. 2025. doi: 10.3847/2041-8213/adf4cd.

K. V. Sokolovsky, Y. Y. Kovalev, A. B. Pushkarev, and A. P. Lobanov. *A&A*, 532:A38, Aug. 2011. doi: 10.1051/0004-6361/201016072.

J. J. Somalwar et al. *ApJ*, 929(2):184, Apr. 2022. doi: 10.3847/1538-4357/ac5e29.

R. Stein et al. *Nature Astronomy*, 5:510–518, Feb. 2021. doi: 10.1038/s41550-020-01295-8.

C. Tadhunter et al. *Nature Astronomy*, 1:0061, Mar. 2017. doi: 10.1038/s41550-017-0061.

A. Tchekhovskoy, B. D. Metzger, D. Giannios, and L. Z. Kelley. *MNRAS*, 437(3):2744–2760, Jan. 2014. doi: 10.1093/mnras/stt2085.

O. Teboul and B. D. Metzger. *ApJL*, 957(1):L9, Nov. 2023. doi: 10.3847/2041-8213/ad0037.

B. Trakhtenbrot et al. *ApJ*, 883(1):94, Sept. 2019a. doi: 10.3847/1538-4357/ab39e4.

B. Trakhtenbrot et al. *Nature Astronomy*, 3:242–250, Jan. 2019b. doi: 10.1038/s41550-018-0661-3.

S. van Velzen et al. *MNRAS*, 529(3):2559–2576, Apr. 2024. doi: 10.1093/mnras/stae610.

J. Wei et al. *arXiv e-prints*, art. arXiv:1610.06892, Oct. 2016. doi: 10.48550/arXiv.1610.06892.

H.-J. Wu et al. *MNRAS*, 514(3):4406–4412, Aug. 2022. doi: 10.1093/mnras/stac1621.

J. Yang et al. *MNRAS*, 462(1):L66–L70, Oct. 2016. doi: 10.1093/mnrasl/slw107.

L. Yang et al. *ApJL*, 993(1):L2, Nov. 2025. doi: 10.3847/2041-8213/ae0caa.

Y. Yao et al. *ApJL*, 955(1):L6, Sept. 2023. doi: 10.3847/2041-8213/acf216.

Y. Yao et al. *ApJL*, 985(2):L48, June 2025. doi: 10.3847/2041-8213/add7de.

W. Yuan et al. *Science China Physics, Mechanics, and Astronomy*, 68(3):239501, Mar. 2025. doi: 10.1007/s11433-024-2600-3.

C. Zhou et al. *ApJ*, 963(1):66, Mar. 2024. doi: 10.3847/1538-4357/ad20f3.

T. Zhou et al. *Phys. Rev. D*, 113(4):043046, Feb. 2026. doi: 10.1103/j8g9-f6hh.